Int. J. Multiphase Flow Vol. 18, No. 4, pp. 541–557, 1992
Printed in Great Britain.

0301-9322/92 $5.00 + 0.00

ANALYSIS OF STRATIFIED/NON-STRATIFIED TRANSITIONAL BOUNDARIES IN INCLINED GAS–LIQUID FLOWS

N. BRAUNER and D. MOALEM MARON
Department of Fluid Mechanics and Heat Transfer, Faculty of Engineering, University of Tel-Aviv, Ramat-Aviv 69978, Tel-Aviv, Israel

(*Received 5 July 1991; in revised form 31 January 1992*)

Abstract—Stability and well-posedness analyses are shown to yield complimentary predictive tools for the stability of stratified gas–liquid flow and the departure to other bounding flow patterns over a wide range of (upward and downward) inclination. The conditions for marginal stability and well-posedness are further shown to coincide with the conditions for stable kinematic and dynamic waves derived from wave theory. A complete stratified/non-stratified transitional boundary is proposed, which shows satisfactory agreement with experimental observations in horizontal and inclined conduits. The observed sensitivity of the departure from the stratified configuration to the flow inclination is well-elucidated, in view of the dramatic effects of inclination on the structure of the stability and well-posedness map. The effects of physical properties, liquid viscosity, phases densities and density differential on the stability and well-posedness map in inclined systems are also explored.

Key Words: stratified flow, inclined, flow pattern transitions, stability, kinematic waves, dynamic waves, well-posedness

1. INTRODUCTION

In exploring the departure from the stratified configuration, the evolution of amplified interfacial disturbances is considered as a precursor to transition. Hence, traditionally the approach of a stability analysis has been employed, either by applying the classical inviscid Kelvin–Helmholtz (K–H) theory (Kordyban & Ranov 1970; Kordyban 1977; Wallis & Dobson 1973) or through a "viscid" analysis, whereby the various shear stresses are accounted for (Lin & Hanratty 1986; Andritsos & Hanratty 1987; Andritsos *et al.* 1989).

Another approach for analyzing the stability of the flow is based on wave-theory. In deriving the characteristics of kinematic and dynamic waves in two-component flow, Wallis (1969) has shown that the relations between the velocities of these two classes of waves govern the stability of the two stratified layers. It has been shown that the condition of equal kinematic and dynamic waves velocities corresponds to marginal stability. Following this approach, Wu *et al.* (1987) determined the stratified/non-stratified transition in horizontal gas–liquid flows.

As shown herein, the above stability analysis is insufficient to yield the complete transitional boundary to the various boundary patterns. Recently, the authors, in attempting to study the stability and transitions in *horizontal liquid–liquid* two-phase flows (Brauner & Moalem Maron 1992a, b), invoked parallel analyses on the stability as well as on the well-posedness of the (hyperbolic) equations which govern the stratified flow. It has been shown that the departure from the stratified configuration is associated with a "*buffer zone*", confined between the conditions derived from stability analysis (a lower bound) and those obtained by requiring well-posedness of the transient governing equations (an upper bound). These two bounds form the basis for the construction of the complete stratified/non-stratified transitional boundary for the various bounding flow patterns. The integrated frame of stability and well-posedness analyses has been found suitable also for horizontal *gas–liquid* systems (Brauner & Moalem Maron 1991). However, as yet, no systematic stability analysis of stratified inclined flow has been reported, a particular focus is required on the effect of inclination.

The purpose of the present study is thus three-fold. First, to frame the general relations between stability and well-posedness on the one hand, and the characteristics of kinematic and dynamic waves on the other. This may bridge between the various approaches which stem from stability

analyses and others based on wave-theory. Secondly, to clarify some of the basic aspects regarding the stability characteristics of *inclined* gas–liquid flows and to explore the relative destabilizing contributions of the two phases. Finally, the various presented analyses are integrated to construct a *complete* stratified/non-stratified transitional boundary in downward and upward *inclined* gas–liquid systems.

2. THEORETICAL ANALYSIS AND CONCEPTS

Referring to an inclined stratified gas–liquid flow and utilizing the average one-dimensional, two-fluid transient formulation, the two continuity equations and combined momentum equation read:

$$\frac{\partial}{\partial t}(\rho_L A_L) + \frac{\partial}{\partial x}(\rho_L A_L u_L) = 0, \tag{1}$$

$$\frac{\partial}{\partial t}(\rho_G A_G) + \frac{\partial}{\partial x}(\rho_G A_G u_G) = 0 \tag{2}$$

and

$$\left[\rho_L(1-\gamma_L)\frac{u_L}{A_L} + \rho_G(1-\gamma_G)\frac{u_G}{A_G}\right]\frac{dA_L}{dh}\frac{\partial h}{\partial t} + (\rho_L - \rho_G)g\cos\beta\frac{\partial h}{\partial x} - \frac{\partial}{\partial x}\left\{\sigma\frac{\frac{\partial^2 h}{\partial x^2}}{\left[1+\left(\frac{\partial h}{\partial x}\right)^2\right]^{3/2}}\right\}$$
$$+ \rho_L\frac{\partial u_L}{\partial t} + \rho_L\gamma_L u_L\frac{\partial u_L}{\partial x} - \rho_G\frac{\partial u_G}{\partial t} - \rho_G\gamma_G u_G\frac{\partial u_G}{\partial x} = \Delta f_{GL}, \tag{3}$$

with

$$\Delta f_{GL} = -\tau_L\frac{S_L}{A_L} \pm \tau_i S_i\left(\frac{1}{A_L} + \frac{1}{A_G}\right) + \tau_G\frac{S_G}{A_G} + (\rho_L - \rho_G)g\sin\beta, \tag{4}$$

where: u_G, u_L denote instantaneous local values for the gas and liquid phases velocities, h stands for the liquid phase depth; γ_G, γ_L are the shape factors which account for a velocity distribution in the two phases; and A, S are the flow cross-section areas and perimeter lengths (functions of h). The shear stresses, τ_G, τ_L and τ_i are expressed in terms of the corresponding friction factors f_G, f_L and f_i. In the framework of quasi-steady modelling of the shear stresses these are to be modelled in terms of the flow variables u_G, u_L, h according to the particular physical situations under consideration. The positive sign in [4] corresponds to a faster gas phase, whereas a negative sign corresponds to a faster liquid phase. In the case of horizontal gas–liquid stratified flows, the gas velocity is practically always much higher than the liquid velocity, whereby the interface is considered as free surface with respect to the liquid phase and as stationary surface with respect to the fast gas phase. In the case of inclined flows, however, it is shown herein that the phases velocities may be comparable and, depending on the particular operational conditions, the velocity of one of the phases may exceed the other. Consequently, "adjustable definitions" for the hydraulic diameters of the two phases ought to be used in the shear stresses modelling as part of the solution procedure. Moreover, for a given downward inclination, the modelling of the fully-developed gas–liquid stratified flow becomes dependent on three parameters (the input flow rates ratio in addition to the Martinelli parameter and inclination). These aspects and others have been detailed recently by the authors with reference to stratified liquid–liquid layers of comparable velocities (Brauner & Moalem Maron 1989, 1992a).

Due to the conceptual link (as shown below) between stability and well-posedness on the one hand and the kinematic and dynamic wave characteristics on the other, the governing transient equations [1–3] are explored along two main routes: stability analysis and the conditions for possessing real characteristics and their relations to the propagation of kinematic and dynamic waves.

2.1. Stability analysis in relation to kinematic and dynamic waves

The conditions for stability are derived by perturbing the linearized transient model equations around a presumed smooth fully-developed stratified flow pattern. This yields a dispersion equation which relates the real wave number, k to the complex wave velocity, $C = \omega/k$. Based on the dispersion equation, the so-called neutral stability conditions are obtained by requiring a zero imaginary part for C, whereby the neutral stable wave number, k_n, and the corresponding wave velocity, C_m are (Brauner & Moalem Maron 1992a):

$$J_G + J_L = 1 + J_\sigma, \qquad [5]$$

with

$$J_\sigma = \frac{\sigma k_n^2}{(\rho_L - \rho_G) g \cos\beta},$$

$$J_G = \frac{U_{Gs}^2}{Dg\cos\beta\,(\rho_L - \rho_G)}\frac{\rho_G}{(1-\epsilon)^3}\frac{\epsilon'}{}\left[\left(\frac{C_m}{U_G} - 1\right)^2 + \left(1 - 2\frac{C_m}{U_G}\right)(\gamma_G - 1)\right],$$

$$J_L = \frac{U_{Ls}^2}{Dg\cos\beta\,(\rho_L - \rho_G)}\frac{\rho_L}{\epsilon^3}\frac{\epsilon'}{}\left[\left(\frac{C_m}{U_L} - 1\right)^2 + \left(1 - 2\frac{C_m}{U_L}\right)(\gamma_L - 1)\right], \qquad [6a]$$

$$C_m = \frac{\dfrac{U_L}{\epsilon}\dfrac{\partial(\Delta F_{GL})}{\partial U_L} - \dfrac{U_G}{(1-\epsilon)}\dfrac{\partial(\Delta F_{GL})}{\partial U_G} - \dfrac{\partial(\Delta F_{GL})}{\partial \epsilon}}{\dfrac{1}{\epsilon}\dfrac{\partial \Delta F_{GL}}{\partial U_L} - \dfrac{1}{(1-\epsilon)}\dfrac{\partial \Delta F_{GL}}{\partial U_G}} \qquad [6b]$$

and

$$\epsilon = \frac{A_L}{A}, \quad \epsilon' = \frac{d\epsilon}{d\tilde{H}}. \qquad [6c]$$

Where $\partial \Delta F_{GL}/\partial(H, U_G, U_L)$ are $\partial \Delta f_{GL}/\partial(h, u_G, u_L)$ at steady conditions H, U_G, U_L with U_{Gs}, U_{Ls} as the superficial phases velocities ($\equiv 4Q/\pi D^2$), and $\sim$ denotes normalized values (areas by D^2 and lengths by D). Note that the l.h.s. of [5] includes the destabilizing contributions of the two phases inertia (relative to gravity) J_L, J_G. These vanish for particular combinations of wave celerity and shape factor related by $C_m/U = \gamma \pm (\gamma^2 - \gamma)^{1/2}$. For instance, for plug flow and a stationary liquid phase ($\gamma_L = 1$, $C_m = U_L$; as conventionally used in previous stability analyses) or for a linear velocity profile in the liquids, $\gamma_L = 4/3$ and $C_m = 2U_L$.

Inspection of [5] and [6] indicates that the structure of [5] is *invariant* with the specific quasi-steady modelling of the wall and interfacial shear stresses, and evolves essentially from the continuity equations and the l.h.s. of the momentum equations. On the other hand, [6] for C_m is directly related to the modelling of the various shear stress terms at steady state (the r.h.s. of the two-fluid momentum equation [4]). In this sense, the form of [5] is general and is affected by the modelling of shear stresses only indirectly through the C_m value. Thus, given different correlations for the shear stresses (e.g. Andreussi & Persen 1987), the general form of [6] provides the corresponding values for C_m.

It is of particular interest to show at this point, that the expression for the wave velocity at neural stability, [6] for C_m, is in fact identical to the definition of kinematic wave velocity, C_k. Starting with the definition of kinematic wave velocity (Wallis 1969)

$$C_k = \left(\frac{\partial U_{Ls}}{\partial \epsilon}\right)_{U_m, \Delta F_{GL}} \qquad [7a]$$

where

$$U_m = U_{Ls} + U_{Gs} = \epsilon U_L + (1-\epsilon) U_G, \qquad [7b]$$

the conditions of quasi-equilibrium of forces, $\Delta F_{GL} = \text{const} = 0$, and constant total flux, U_m, are to be maintained in [7a]:

$$d(\Delta F_{GL}) = \frac{\partial \Delta F_{GL}}{\partial U_G} dU_G + \frac{\partial \Delta F_{GL}}{\partial U_L} dU_L + \frac{\partial \Delta F_{GL}}{\partial \epsilon} d\epsilon = 0 \quad [8a]$$

and

$$dU_{Ls} = -dU_{Gs}. \quad [8b]$$

Combining [7b] and [8b] yields dU_L and dU_G (in terms of dU_{Ls} and $d\epsilon$), which when substituted into [8a] result in an expression for the derivative of the liquid flux with respect to concentration, [7a], in terms of U_L, U_G, ϵ, which is identical to [6b].

Thus, the neutral stable wave actually represents a continuity wave and its characteristic velocity can be determined either by stability analysis or via the derivative of the liquid flux with respect to its *in situ* hold-up (concentration). Clearly, both the neutrally stable and continuity waves are based on the steady momentum equation. In view of this relationship between neutral stable and kinematic waves, and for the sake of further interpretations, the general dispersion equation [derived in Brauner & Moalem Maron (1992a)] is rearranged now in terms of C_k ($\equiv C_m$):

$$C^2 - \left[2V_0 - \frac{i}{k} V_1\right] C + V_2^2 - \frac{i}{k} C_k V_1 = 0, \quad [9]$$

where

$$V_0 = \frac{\gamma_L \rho_L \dfrac{U_L}{A_L} + \gamma_G \rho_G \dfrac{U_G}{A_G}}{\dfrac{\rho_L}{A_L} + \dfrac{\rho_G}{A_G}}, \quad [10a]$$

$$V_1 = \frac{\dfrac{1}{A_G}\dfrac{\partial \Delta F_{GL}}{\partial U_G} - \dfrac{1}{A_L}\dfrac{\partial \Delta F_{GL}}{\partial U_L}}{\dfrac{\rho_L}{A_L} + \dfrac{\rho_G}{A_G}}, \quad [10b]$$

$$V_2^2 = \frac{\gamma_L \rho_L \dfrac{U_L^2}{A_L} + \gamma_G \rho_G \dfrac{U_G^2}{A_G} - \dfrac{(\Delta \rho g \cos \beta + \sigma k^2)}{A_L'}}{\dfrac{\rho_L}{A_L} + \dfrac{\rho_G}{A_G}}. \quad [10c]$$

Here, V_0 represents a weighted mean velocity of the two phases and V_1 is a damping parameter due to the shear stresses. [Based on the shear stresses modelling, as detailed by Brauner & Moalem Maron (1992a), it can be shown that V_1 attains always a positive value, independent of the relative velocity between the two phases.]

The relation of the general dispersion equations [9] to *dynamic waves* is derived here by recalling that a *pure* dynamic wave occurs whenever the net force on the flowing fluids is produced only by a concentration gradient (and is independent of the *in situ* concentration). In this case, the r.h.s. of the combined momentum equation [4], which is a function of the *in situ* concentration, is to be ignored, whereby Δf_{GL} is considered as identically zero. Thus, the general dispersion equation [9], with $V_1 = 0$, becomes

$$C_d^2 - 2V_0 C_d + V_2^2 = 0,$$

where

$$C_d = V_0 \pm \sqrt{V_0^2 - V_2^2}. \quad [11]$$

Substituting V_2^2 from [10c] into [11] yields the dynamic wave velocity:

$$c_d \equiv C_d - V_0 = \pm \left\{ \left(\gamma_L \rho_L \frac{U_L}{A_L}\right)^2 + \left(\gamma_G \rho_G \frac{U_G}{A_G}\right)^2 + 2\left(\gamma_L \gamma_G \rho_L \rho_G \frac{U_L U_G}{A_L A_G}\right) + \left[\frac{\rho_L}{A_L} + \frac{\rho_G}{A_G}\right]\left[\gamma_L \rho_L \frac{U_L^2}{A_L} - \gamma_G \rho_G \frac{U_G^2}{A_G} + \left(\frac{\Delta\rho g \cos\beta + \sigma k^2}{A_L'}\right)\right]\right\}^{1/2} \left(\frac{\rho_L}{A_L} + \frac{\rho_G}{A_G}\right). \quad [12]$$

Here, c_d is the dynamic wave velocity relative to the weighted mean velocity. Equation [12] (or simply [11]) implies that a stable dynamic wave is obtained provided ($V_0^2 > V_2^2$):

$$\tilde{\rho}_L U_L^2 \gamma_L(\gamma_L - 1) + \tilde{\rho}_G U_G^2 \gamma_G(\gamma_G - 1) - (\gamma_L U_L - \gamma_G U_G)^2 + \frac{D}{\rho_{GL}}[(\rho_L - \rho_G)g\cos\beta + \sigma k^2] \geq 0; \quad [13a]$$

where

$$\tilde{\rho}_L = 1 + \frac{\rho_L}{\rho_G}\frac{\tilde{A}_G}{\tilde{A}_L}, \quad \tilde{\rho}_G = 1 + \frac{\tilde{A}_L}{\tilde{A}_G}, \quad \rho_{GL} = \frac{\tilde{A}_L'}{\tilde{A}_G \tilde{A}_L}\frac{\rho_G \rho_L}{\frac{\rho_G}{\tilde{A}_G} + \frac{\rho_L}{\tilde{A}_L}}. \quad [13b\text{–}d]$$

Note, however, that a *pure* dynamic wave may be physically realized in inviscid flows. In a viscid flow system, the wave characteristics may be related to those of pure dynamic and kinematic waves by introducing $V_2^2 = V_0^2 - c_d^2$ from [11] into the general wave dispersion equation, [9], to yield

$$c^2 - c_d^2 + \frac{i}{k} V_1 (c - c_k) = 0$$

where

$$c = C - V_0, \quad c_k = C_k - V_0. \quad [14]$$

In view of [14], it is easily shown that at neutral stable conditions, the wave velocity is equal to both the kinematic and dynamic waves velocities, $c = c_k = c_d$. Substituting $c = c_r + ic_i$ into [14], results in the wave frequency and wave amplification, in identical forms to those by Wallis (1969):

$$\omega_r \equiv \frac{C_r}{k} = \frac{V_1^2}{4}\left(\frac{C_r}{c_r}\right)^2 \left(\frac{c_k^2 - c_r^2}{c_r^2 - c_d^2}\right) \quad [15a]$$

and

$$\omega_i \equiv \frac{C_i}{k} = \frac{V_1}{2}\left(\frac{c_k}{c_r} - 1\right). \quad [15b]$$

Equations [15a, b] indicate that the locus for which the kinematic wave velocity is equal to that of the dynamic wave $C_k \equiv C_m = C_d$ represents neutral stable wave modes. Indeed, equating C_d from [12] to $C_k (= C_m)$, again renders the condition derived for neutral stability in [5]. Stable modes are obtained for $c_k^2 < c_r^2 < c_d^2$, whereas for unstable modes to exist it is required that $c_k^2 > c_r^2 > c_d^2$ (since $V_1 > 0$). Hence, it is the relation between kinematic and dynamic wave velocities which essentially determines the stability, since $c_k^2 > c_d^2$ corresponds to unstable modes, whereas modes with $c_d^2 > c_k^2$ are attenuated.

In extracting the conditions for the stable or unstable modes from [15a, b], it should be emphasized that ω_r and ω_i are expressed in terms of waves velocities relative to the weighted mean velocity and, therefore, c_k, c_d and c_r may attain negative values. Thus, the condition for an unstable mode, e.g. $c_k^2 > c_d^2$, is equivalent to $C_k > C_d$ when both c_k, c_d are positive, whereas for negative c_k, c_d the conditions becomes $C_k < C_d$. In both cases, however, this means that in terms of absolute relative velocities, the kinematic wave exceeds the dynamic wave, $|C_k - V_0| > |C_d - V_0|$, for an unstable mode. For a stable mode, the absolute relative velocity of the dynamic wave exceeds that of the kinematic wave.

2.2. *Well-posedness in relation to dynamic waves*

In two-phase flow problems, complex characteristics (ill-posed initial-value problem) may not necessarily imply an incorrect formulation, but may be attributed to physical instability of the assumed flow configuration. The test for reality of characteristics on the transient equations [1]–[3] is carried out around the initial condition of fully-developed stratified solution. The condition under which the characteristic roots are real is (Brauner & Moalem Maron 1992a)

$$\tilde{\rho}_L U_L^2 \gamma_L(\gamma_L - 1) + \tilde{\rho}_G U_G^2 \gamma_G(\gamma_G - 1) - (\gamma_L U_L - \gamma_G U_G)^2 + \frac{D}{\rho_{GL}}[(\rho_L - \rho_G)g \cos\beta + \sigma k^2] \geqslant 0. \quad [16]$$

The identity between [16] and [13a] for a stable dynamic wave, indicates that the region of well-posedness coincides with that of stable dynamic waves, $c_d^2 > 0$. In the region where $c_d^2 < 0$, all waves modes are unstable and their evolution, as formulated by the initial value set of [1]–[3] is ill-posed. As the stability condition for inviscid flows ($\Delta f_{GL} \equiv 0$) is equivalent to that of pure dynamic waves, the well-posedness condition is actually equivalent to the classical (inviscid) K–H stability condition.

2.3. *Relations between stability, well-posedness and kinematic and dynamic wave characteristics*

For each combination of (U_{Gs}, U_{Ls}), the range for amplified wave numbers is obtained by solving [5] and [6] for k_n, while [16] is also solved for $k = k_{rc}$, below which ($k < k_{rc}$) the characteristic roots are complex. For $0 < k < k_n$, the variation of the amplification with the wave number ($kC_i = k\mathrm{Im}\{C\}$ vs k) is obtained by the general dispersion equation and presented in figure 1 for slightly inclined flow. For a certain combination of (U_{Gs}, U_{Ls}) as in curves (c), and in the range of $0 < k < k_n$, where the stabilizing effect of surface tension is relatively small, the disturbances are amplified and hence a wavy interfacial structure develops. For these unstable wave modes, the square of the kinematic wave velocity exceeds that of the corresponding pure dynamic wave, $c_k^2 > c_d^2$ (all velocities are relative to the weighted mean velocity). On the other hand, $c_k^2 < c_d^2$ for all the stable wave modes, $k > k_n$. At each wave mode, the square of the wave propagation velocity, c_r^2, lies between the kinematic and dynamic bounds.

It is also worth noting that for a specified (U_{Gs}, U_{Ls}) set, c_k is independent of the wave number, k, and is equal to the neutral stable wave velocity at $k = k_n$ (and $k = 0$). The dynamic wave velocity,

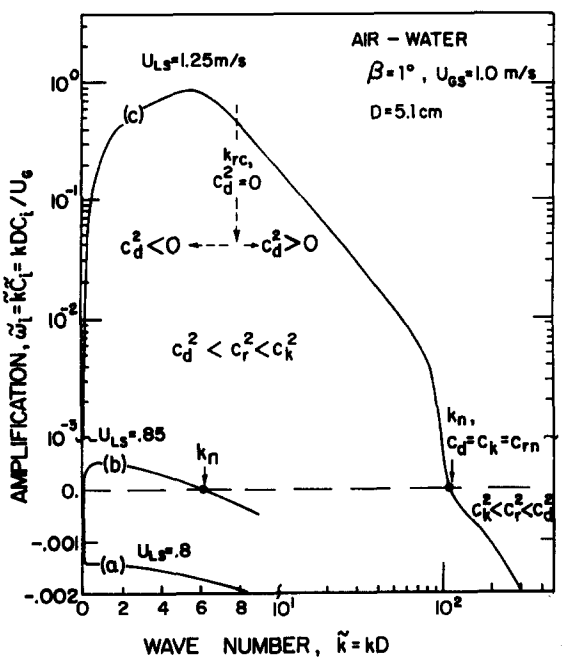

Figure 1. Effect of liquid flow rate on the range of amplified wave modes and the corresponding amplification.

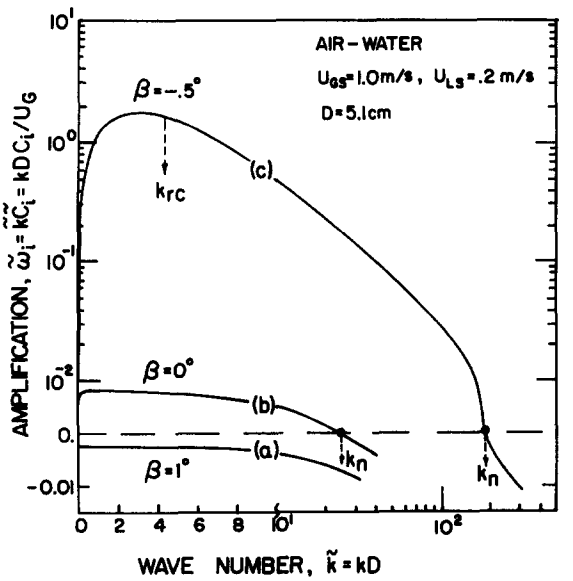

Figure 2. Effect of flow inclination on the range of amplified wave modes and the corresponding amplification.

on the other hand, varies with the wave number. Its square is negative for $k < k_{rc}$, identically zero at $k = k_{rc}$ and becomes positive for $k > k_{rc}$, as marked in figure 1. At the particular value of $k = k_n$, all the characteristic waves velocities are equal, $c_k = c_d = c_m$.

In view of the typical curve (c) of figure 1, for all $k < k_{rc}$, an unstable smooth stratified flow is consistently predicted by both stability and reality of characteristics analyses with $c_d^2 < 0$. However, for any $k_{rc} < k < k_n$, while the governing equations [1]–[3] are well-posed as an initial-value problem, they are still expected to develop a wavy structure. It is to be emphasized that the value of k_{rc} is always within the amplified range, $k_{rc} < k_n$. This has been rigorously shown with reference to general two-fluid liquid–liquid systems (Brauner & Moalem Maron 1992a). As a corollary, it can be stated that the condition of an unstable dynamic wave or ill-posedness is sufficient to indicate instability, whereas the condition of $c_d^2 > 0$ or well-posedness is necessary, but insufficient, to ensure stability.

Clearly, the range of amplified waves, $k < k_n$, varies depending on the (U_{Gs}, U_{Ls}) combinations, as demonstrated in figure 1. For a particular combination of (U_{Gs}, U_{Ls}), as represented by curve (b), the amplified range almost diminishes $(\omega_i, k_n \rightarrow 0)$, while for the conditions of curve (a), for instance, all wave modes are stable.

As figure 1 relates to the effects of the flow rates of the phases, figure 2 includes typical trends for the effect of flow inclination at specified operational conditions, $U_{Gs} = 1$, $U_{Ls} = 0.2$ m/s. For these conditions and in a horizontally levelled tube, $\beta = 0°$, a relatively limited range of weakly amplified (unstable) wave modes just appear. However, all of the growing wave modes are found to be well-posed $(c_d^2 > 0,\ c_d^2 < c_r^2 < c_k^2)$. As the flow is slightly inclined downward, $\beta = 1°$, all the unstable wave modes disappear and the flow becomes smoothly stable for the entire range of wave numbers $(c_d^2 > 0, c_k^2 < c_r^2 < c_d^2)$. On the other hand, inclining the flow slightly upward, $\beta = -0.5°$, results in a drastic increase in both the range of amplified wave numbers and the corresponding amplification. Moreover, a range of ill-posed wave modes also appears $(0 < k < k_{rc}$, for which $c_d^2 < 0)$. Thus, in view of figure 2, the flow inclination has a dramatic effect on the stability of the flow, in the sense that a very slight downward or upward inclination can stabilize or destabilize the stratified flow configuration. However, the impact of a small upward inclination on the stability characteristics is significantly more pronounced. As shown below, this behaviour forms the basis for elucidating the stratified/non-stratified flow patterns transitions observed in upward and downward inclined flows.

3. STABLE STRATIFIED FLOW BOUNDARIES IN INCLINED SYSTEMS

Based on the stability and well-posedness analyses discussed in section 2, the limiting boundaries for stable stratified flows are defined herein. These boundaries are then utilized for constructing a complete stratified/non-stratified transitional line to the various bounding flow patterns (slug, psuedo-slugs and annular flows).

3.1. Stability of the well-posedness map: "zero neutral stability" and "zero real characteristics" lines

As is shown in figures 1 and 2, for a given inclination, there exists a particular combination (U_{Gs}, U_{Ls}) for which the range of amplified waves diminishes, $k_n \rightarrow 0$. In searching for all combinations of (U_{Gs}, U_{Ls}) for which $k_n \rightarrow 0$, the so-called "*zero neutral stability*" line (ZNS) is obtained (by [5] and [6]). This boundary confines all possible *smooth* stratified flows. The locus of the curve itself represents the departure from the *smooth* stratified structure. For any operational set (U_{Gs}, U_{Ls}) outside the $k_n = 0$ boundary, the linear stability analysis predicts exponential growth with time for a finite range of wave numbers, $0 \leqslant k \leqslant k_n$. The growth of disturbances in this region may either be damped, (due to non-linear effects) and thus result in "stable wavy" stratified flow, or may result in a different flow configuration (due to bridging, for instance).

In parallel to the ZNS boundary defined by $k_n = 0$, a "*zero real characteristics*" boundary (ZRC) is constructed by searching for all combinations of (U_{Gs}, U_{Ls}) which yield (by [16]) real characteristics for $k_{rc} = 0$. The ZRC curve confines the region of operational conditions for which well-posedness is ensured for all wave modes.

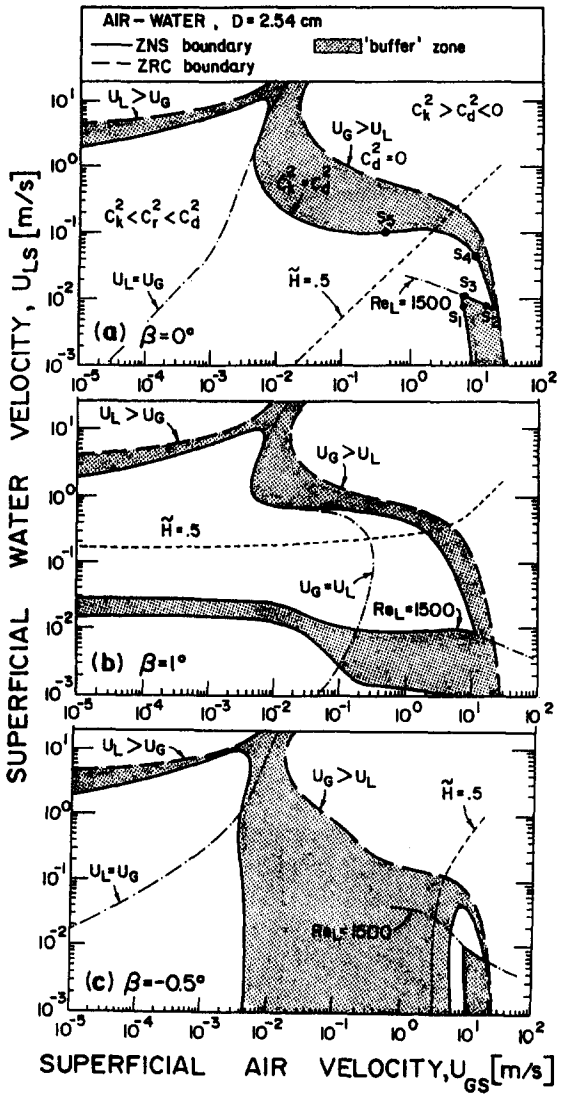

Figure 3. SWP map for air–water horizontal and inclined systems.

The ZNS and ZRC boundaries constitute what is called herein a "*stability and well-posedness (SWP) map*", as presented in figure 3(a–c) for horizontal and downward/upward inclined air–water flows. Generally, the ZRC boundary is composed of two branches, the left one corresponds to $U_L > U_G$ while along the right one $U_G > U_L$. The existence of two branches indicates the multiplicity of solutions, which becomes even more complicated along the ZNS boundary; it is also due to the discontinuities which evolve from laminar/turbulent flow regime transitions in either of the two phases. While point S_1 in figure 3(a) represents the limiting conditions for a smooth stratified *laminar* water layer, at point S_2 or S_3, the flow restabilizes as the water layer becomes turbulent (at $Re_L = 1500$). With a further increase in either the gas or liquid rates point S_4 is reached, where the *turbulent* smooth liquid layer now attains a neutral stable situation. Thus, the region between points S_2–S_3–S_4 corresponds to a stable turbulent liquid layer. As shown in figure 3(a–c), the multiplicity of solutions becomes more pronounced in inclined flows. The structure of the SWP map in figure 3(a) for a horizontal air–water system has been found to be typical of all *horizontal* flows of air–viscous liquids over wide ranges of liquid viscosity and tube diameter. [A wide range of U_{Gs} is included in figure 3(a–c) to show some general features of SWP maps.] In figure 3(a) the instability characteristics are further discussed with reference to the characteristics of the kinematic and dynamic waves derived in section 2. In the smooth stratified region confined by the ZNS boundary, $c_d^2 > c_k^2$ and $c_k^2 < c_r^2 < c_d^2$ for all wave modes; while along the ZNS itself, $c_d^2 = c_k^2$ for the

limit of long waves ($k = k_n \to 0$). Clearly, for all other modes, $c_d^2 > c_k^2$ certainly prevails along the ZNS. In the ill-posed region beyond the ZRC line, there exist a range of unstable dynamic waves, $0 < k < k_{rc}$, for which $c_d^2 < 0$ and $c_k^2 > c_d^2$. Along the ZRC boundary, $c_d^2(k_{rc} \to 0) = 0$, and the dynamic (long) waves are marginally stable, while all other dynamic waves modes are certainly stable. Between the limits of the ZNS and ZRC boundaries (shaded areas), $c_d^2 > 0$ for all wave modes, including those unstable modes for which $c_k^2 > c_d^2$ (and $c_d^2 < c_r^2 < c_k^2$).

The ideas and interpretations above, detailed with regard to the horizontal system of figure 3(a), prevail basically in inclined flow also, although the limiting ZNS and ZRC boundaries may demonstrate entirely different structures. The first point to note is the significant effect of inclination on the liquid layer velocity relative to the gas velocity. A downward inclination accelerates the liquid layer, whereby a region of $U_L > U_G$ (left of the $U_L = U_G$ line) appears within the practical range of gas–liquid rates. On the other hand, with upward inclination the relative gas to liquid velocity becomes much higher and the equal velocities line moves left, to a region of extremely low gas rates. These pronounced changes in the phase velocities are accompanied by a corresponding drastic variation in the liquid layer thickness. For given gas and liquid rates, inclining the flow downwards, results in a thinner liquid layer, which is practically insensitive to the gas rate over a wide range. On the other hand, an upward inclination results in a drastic thickening of the liquid layer with high sensitivity to the gas rate. The dramatic changes in the flow geometry, phase velocities and their ratio affect, in view of [5], [6] and [16], the ZNS and ZRC locations. For instance, the small "side" buffer zone in figure 3(a), which corresponds to an unstable laminar liquid layer and is obtained only at high gas rates at $\beta = 0$, penetrates towards much lower gas rates in downward inclination, figure 3(b). Note that, as the liquid rate is increased in this zone (at a specific gas rate), the flow stabilizes "discontinuously" due to laminar/turbulent flow regime transition in the liquid layer. In comparison, with inclining the flow upward, figure 3(c), a large unstable zone (shaded area) extends to relatively low liquid rates over a wide range of gas rates. At high gas rates, a limited bell-shaped stratified zone still prevails at this particular slight upward inclination. At higher inclinations, the resulting variations in the steady stratified solution (U_L, U_G, H) are even higher, affecting stronger effects on the stability and well-posedness map.

3.2. Construction of the stratified/non-stratified transitional boundary

The general implication of the ZNS and ZRC lines, is in defining *three zones*; the area within the ZNS boundary, is well-understood to be the stable *smooth* stratified zone. Beyond the ZRC boundary, the complex characteristics imply that the governing equations of the stratified flow configuration cannot accommodate for the time and space variations associated with a certain range of amplified wave modes. Thus, while the ZNS boundary may represent a preliminary transition to a wavy interfacial structure, the ZRC boundary, which is within the wavy unstable region, represents an upper bound for the existence of a wavy stratified configuration, beyond which another flow pattern prevails. It is worth noting, that the stable smooth stratified zone, as defined by the ZNS line, is always a subzone confined within the well-posed region.

The "*buffer*" region between the ZNS and ZRC lines is characterized by the evolution of amplified interfacial waves, the growth of which, as governed by the variation of (h, u_G, u_L) in space and time, is still well-posed. Whether these disturbances trigger a departure from the stratified configuration (due to blockage) depends on the relative layer thicknesses. For if $\tilde{H} = H/D \simeq 0.5$ to 1, it is likely that the evolution of the interfacial disturbances on the liquid layer will result in the tube blockage. Thus, when the *entry* from the smooth into the "buffer" zone (along the ZNS boundary) is associated with a relatively thick liquid layer [above the $\tilde{H} = 0.5$ line, as at point S_6 in figure 3(a)], the ZNS line which, in general, represents the transition to a disturbed wavy pattern, will also predict the conditions for the development of other flow patterns. On the other hand, when the entry to the "buffer" zone (along the ZNS boundary) occurs with a relatively thin liquid layer (below the $\tilde{H} \simeq 0.5$ line, as points S_1–S_4), the ZNS line is associated with the development of wavy stratified flow, but it plays no role in predicting the transition to other patterns. In this case, the transition to other flow configurations may be "delayed" and predicted by the ZRC boundary, as long as the relative liquid layer thickness, H/D, remains small *in* the "buffer" zone. As the relative liquid layer becomes of the order of the conduit radius, $H/D \approx 0.5$, *within* the "buffer" region, the disturbed interface may trigger flow pattern transition, this time *within* the "buffer" zone in the

vicinity of the $H/D \approx 0.5$ line. It is to be emphasized at this point, that although the structure of the SWP map varies dramatically with inclination (and physical properties), the principles of constructing the complete stratified/non-stratified transitional boundary are essentially applied along the same guidelines: along the ZNS boundary for $\tilde{H} > \tilde{H}_{crit}(=0.5)$, following $\tilde{H} = \tilde{H}_{crit}$ within the "buffer zone" and joining the ZRC track in the region of $\tilde{H} < \tilde{H}_{crit}$. Clearly, $\tilde{H}_{crit} = 0.5$ avoids a complicated non-linear stability analysis which is required to determine whether the growing waves in the "buffer" wavy region will indeed reach the upper tube wall and thus end in a different flow pattern. Note further, that the $H/D \approx 0.5$ section is not to be confused with the annular/slug transition (which is clearly beyond the stratified zone) and is determined by the limiting conditions of the annular configuration (Brauner & Moalem Maron 1992b).

Based on these guidelines, the resulting stratified/non-stratified transitional boundaries corresponding to figure 3(a–c) are constructed (for practical range of gas rates) in figure 4(a–c). For clarity, the predicted stable stratified smooth (S) and stratified wavy (SW) zones are shaded differently and the transitional boundaries sections are in bold.

3.3. Stratified/stratified–dispersed transition: SD boundary

At sufficiently low gas/liquid input ratio, gas bubbles which accumulate at the upper tube cross-section, may still maintain their identity and thus the system may demonstrate a stratified–dispersed flow pattern. The gas phase may remain dispersed as a swarm of bubbles, provided the bubbles are small enough for the surface tension forces to overcome those due to buoyancy. A transitional criterion for stratified–dispersed flow has been proposed recently (Brauner & Moalem Maron 1992b) and is denoted in figure 4(a–c) as the SD boundary.

The SD line is of relevance for complete construction of the stratified/non-stratified boundary only when it crosses the zone of stable stratification. In view of figure 4(a, b), the stratified–dispersed pattern in gas–liquid systems appears as a very small subzone of the stratified configuration and for sufficiently large tubes it is usually below the practical range of gas/liquid input ratios. For smaller tube diameters, larger stratified–dispersed zones are predicted. For upward inclination, figure 4(c), the SD boundary is outside the stable stratified region, implying that a stratified–dispersed pattern is not expected to develop. It is of interest to note that in liquid–liquid systems, extended stratified–dispersed zones may appear, at either the top or bottom of the conduit cross-section, due to the reduced density differential in liquid–liquid systems (Brauner & Moalem Maron 1992b; Brauner 1990). In gas–liquid systems, however, the stratified–dispersed pattern when observed (in small tubes) has usually been identified as part of the bubble flow zone (Brauner & Moalem Maron 1992c).

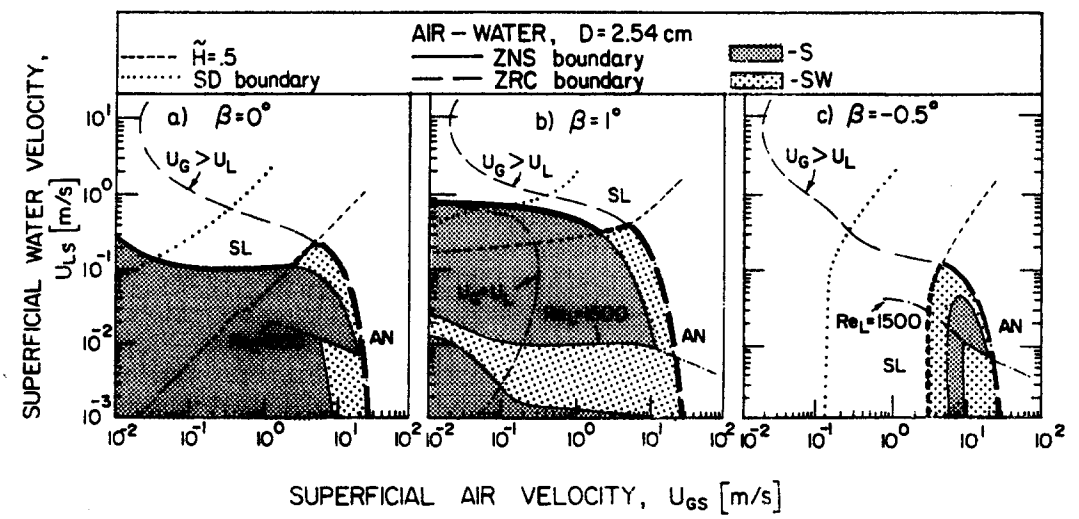

Figure 4. Construction of the stratified/non-stratified transitional boundary.

4. DISCUSSION

The guidelines formulated in section 3 for constructing the complete stratified/non-stratified transitional boundary are now to be tested in view of the available experimental data for inclined air–water systems. The effects of the physical properties of the fluids and their relative destabilizing contributions in inclined flows are also evaluated and discussed.

4.1. Comparison with experiments

Figures 5(a–d) and 6(a–f) present typical comparisons of the proposed stratified/non-stratified transitional boundary with available experimental data for air–water flows in 2.54 and 5.1 cm dia over a wide range of downward/upward inclinations (Mandhane *et al.* 1974; Shoham 1982).

Inspection of figures 5(a–d) and 6(a–f) shows that in the region of relatively thin liquid layers, $\tilde{H} < 0.5$, the experimental transition data consistently follows the trend of the ZRC boundary. It is to be emphasized that for horizontal flow [figure 6(a)] the ZNS and ZRC boundaries are rather close to each other in this region and the data may seem to follow either of these. In inclined flow these two boundaries diverge significantly. However, the transitional data stick to the ZRC line, although this boundary now lies deep in the unstable smooth (or stratified wavy) region. This reinforces the dominant role of the well-posedness boundary in predicting the flow pattern transition in the region of relatively thin liquid layers as elucidated in section 3.2.

The characteristic shape of the ZRC line is preserved over a wide range of downward inclinations. In upward inclinations the ill-posed zone has already started penetrating towards lower liquid rates at $\beta = -0.5°$. At $\beta = -1°$ (and steeper upward inclinations), the well-posed

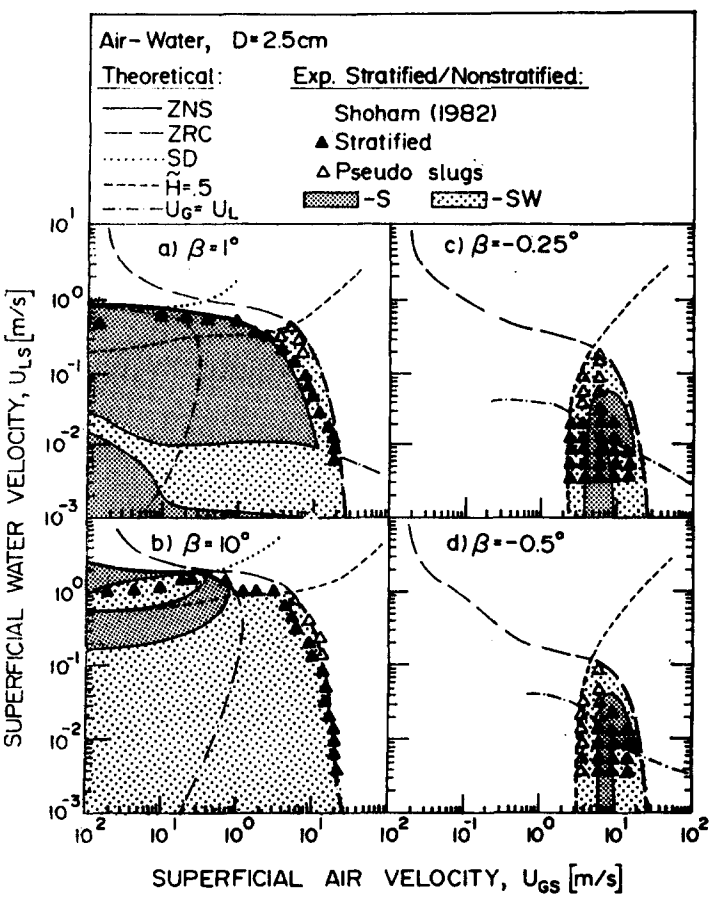

Figure 5. Stratified/non-stratified transition in inclined air–water systems—comparison with experiment, $D = 2.5$ cm (▲, stratified; △, pseudo-slugs).

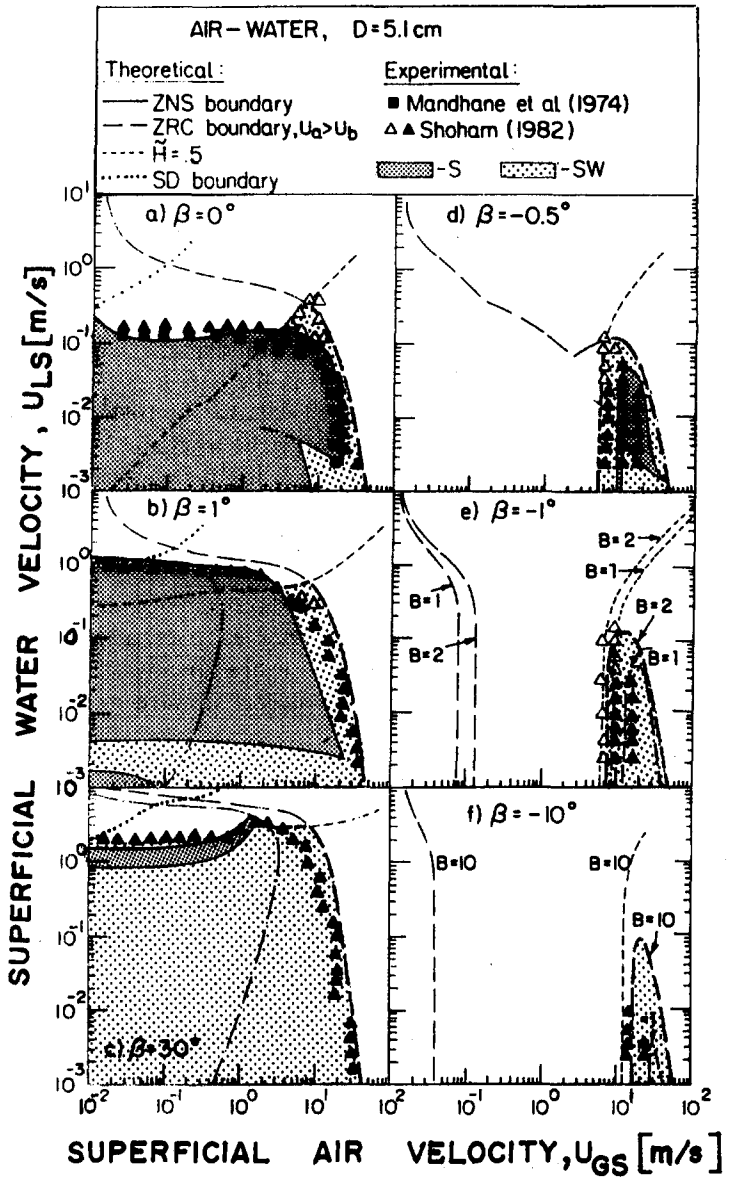

Figure 6. Stratified/non-stratified transition in inclined air–water systems—comparison with experiment, $D = 5.1$ cm.

region is seen to split into two separate regions. The first is entirely unstable and corresponds to low gas rates with $H \gg 0.5$, while the second at high gas rates (confines a stable subzone) is bell-shaped along which $\tilde{H} < 0.5$, and is thus the relevant one to transition prediction. These two well-posed zones are apparently separated as they merge at lower liquid rates [out of the practical range of figure 6(e, f)]. The ZNS line, as marked in figure 5(c, d), also form smaller bell-shaped zones of stable smooth stratified flow.

According to the proposed transitional boundary, the role of the ZRC line in predicting transition ends at the intersection with the $\tilde{H} = 0.5$ line. From this point, the departure from a stable stratified configuration is expected, first along the $\tilde{H} = 0.5$ line in the wavy "buffer" zone and then along that section of the ZNS line for which $\tilde{H} > 0.5$. This is clearly the case in figures 5(a, b) and 6(a, b). In this case the complete stratified/non-stratified boundary is indeed composed of the three sections. However, when almost all the stable region confined by the ZNS line corresponds to $\tilde{H} < 0.5$, as in figures 5(c, d) and 6(c, d), the ZNS line becomes irrelevant in

predicting a departure from a stratified configuration. Clearly, in this case, the transitional boundary follows first the ZRC line for $\tilde{H} < 0.5$ and then the $\tilde{H} = 0.5$ line throughout the "buffer" zone. Another possible situation is that in figure 6(e, f), where the critical layer thickness line, $\tilde{H} = 0.5$, falls in the ill-posed region, in which case the flow pattern transition is entirely predicted by the ZRC location. Note also that the SD boundary, which is included in figures 5(a–d) and 6(a–f), may sometimes reduce the predicted stable stratified zone to some extent [as in figure 5(b)].

It is of further interest to refer to the data which relates to the so-called pseudo-slug pattern [denoted sometimes as large-wave stratified flow or wavy annular flow; Δ in figures 5(a–d) and 6(a–f)]. The pseudo-slug region is characterized by high-amplitude roll waves which extensively wet the upper tube walls, without causing the pressure fluctuations typical to a slug pattern. Inspection of the data reveals that the regions of pseudo-slugs develop within the herein predicted "buffer" region around $\tilde{H} = 0.5$. Indeed thick wavy layers bear the conditions for large-amplitude waves and extensive wetting of the upper wall, hence psuedo-slugs. Clearly, large-amplitude waves are more likely to cause pseudo-slugs in small diameters than in large diameters.

In upward inclinations, the ZRC boundary predicts too fast a shrinkage of the stratified zone with increasing inclination using $f_i = f_G$. However, its comparison with the data significantly improves when amplification of the interfacial shear factor is considered [$f_i = BF_G$, $B > 1$, figure 6(e, f)]. Indeed, augmentation of the interfacial shear factor is expected due to the relatively thick wavy liquid layer associated with upward inclination (particularly along the left part of the ZRC "bell" closer to $\tilde{H} = 0.5$).

In view of figures 5(a–d) and 6(a–f), it is shown that, in spite of the variety of situations which appear at the different inclinations, the general guidelines for constructing the stratified/non-stratified transitional boundary are essentially maintained.

4.2. Effect of liquid phase viscosity

No experimental data is available for gas–viscous liquid flows in inclined tubes. However, as the present analytic approach has been shown to be a reasonable predictive tool, it would be valuable to present the combined effects of liquid viscosity and inclination as predicted by the present analyses.

Figure 7(a–f) demonstrates the SWP maps for varying liquid viscosity and inclination. Comparing figure 7(a–f) with figure 3(a–c) for the same inclination indicates reduced regions of both stable smooth stratification and well-posedness with increasing the liquid viscosity. The reduced "buffer" zone and the thickening of the liquid layer in viscous liquids render an extended range of operational conditions where the ZNS boundary (for $\tilde{H} > 0.5$) controls the departure from stratified configurations. Thus, while with increasing inclination the role of the ZNS boundary diminishes [figures 5(a–d) and 6(a–f)], it may become of importance in determining transitions in high viscous liquids. Hence, it may be stated that increased liquid viscosity moderates the effects of flow inclination on the SWP map. Also, expansion of the stratified–dispersed subzone with increasing liquid viscosity on account of the stratified zone is to be considered. For instance, for $\beta = -0.5°$ at 1000 cP, figure 7(f) indicates that practically only the stratified–dispersed pattern is to be expected.

4.3. Effect of density

For completeness, the effect of the phases densities and the associated density differential on the SWP map are demonstrated in figure 8(a–d). Comparing figure 8(a) with figure 3(a) indicates that, for horizontal flow, the reduction in the density differential (from ~ 1 to ~ 0.8) by decreasing the liquid density results in only minor changes. However, figure 8(b) shows that when the same density differential reduction is due to an increase in the gas density, the stability characteristics are influenced significantly. The main effects of increasing ρ_G are the increase in the liquid rates and the decrease in the gas rates for which stable stratification can be maintained. This implies that in high-pressure systems, for instance, while the stratified/slug transition is delayed to higher liquid rates, the stratified/annular transition is expected at lower gas rates.

It should be noted also that utilizing the modified coordinates $(\rho_G/\Delta\rho)^{1/2}U_{Gs}$ and $(\rho_L/\Delta\rho)^{1/2}U_{Ls}$ instead of U_{Gs} and U_{Ls} significantly reduces the effect of the gas density on the location of the stratified/annular transtion. Therefore, such a presentation may be an advantage in scaling

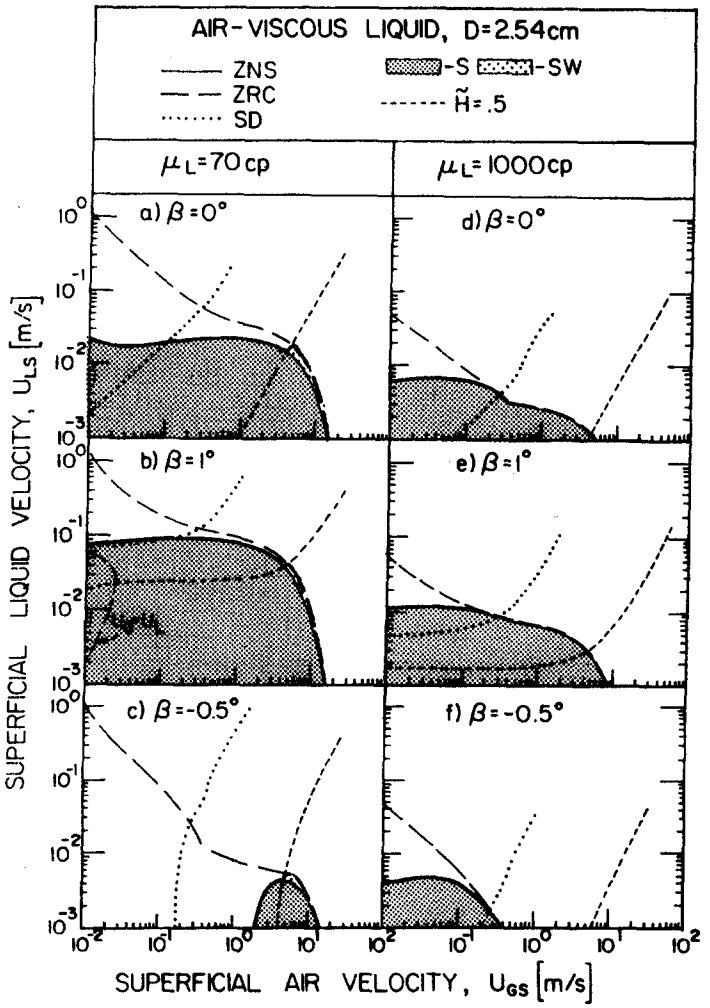

Figure 7. Effect of liquid viscosity on the transitional boundaries in inclined systems.

the stratified/annular transition to high-pressure systems. However, no universal structure for the complete SWP maps and the stratified/non-stratified transition boundary can be obtained.

4.4. Identification of liquid-controlled or gas-controlled stability

In [5] the gas and liquid destabilizing terms, J_G and J_L respectively, represent the combined effects of inertia (as evolve from the l.h.s. of [1]–[3]) and viscosity (via C_m, as evolves from the r.h.s. of [3]). Obviously, in the range of relatively low gas rates, which usually corresponds to the stratified/slug transition, the liquid destabilizing term is expected to be the dominating one, $J_L > J_G$. This corresponds to "*liquid-controlled*" transition. For sufficiently high gas rates, along the stratified/annular transition, the contribution of the gas phase term may overtake that of the liquid layer, $J_G > J_L$ and thus "*gas-controlled*" transition may be considered. This is demonstrated in figure 9(a, b) for various physical systems and inclinations. Note that figure 9(a) is calculated along those sections of the ZNS curves, which have been found relevant for transition prediction in figures 5(a–d) and 6(a–f) (along the other ZNS boundaries within the shaded stable stratified region, J_L is even higher). It is clear from figure 9(a) that for an air–water system the liquid phase dominancy, J_L, is consistently preserved for horizontal as well as for downward inclined flows, except at very high gas rates in the horizontal case. In inclined flows, the ZNS boundary does not extend to high gas rates, while it becomes irrelevant for transition prediction for steep inclinations. Thus, for an inclined air–water system, the transition (when determined by linear stability) is practically "liquid-controlled". As the liquid viscosity is increased [figure 9(b)], the range of "*gas controlled*" stability and transition becomes more significant.

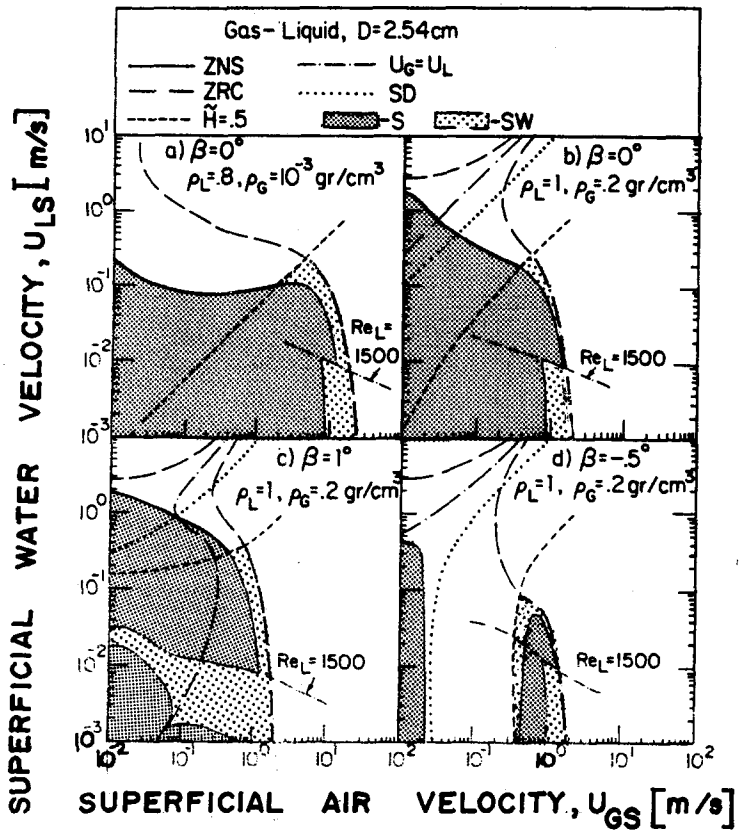

Figure 8. Effect of the fluids densities and density differential on the transitional boundaries.

It is of importance to emphasize that previous studies related to the stratified/slug flow pattern transition assumed, in fact, a "*gas-controlled*" transition by unjustifiably ignoring the liquid destabilizing contribution totally. As their modelling is essentially based on the gas contribution, which plays a minor role along the stratified/slug boundary, a reasonable comparison with experiments required the insertion of empirical correction coefficients. For instance, Wallis & Dobson (1973), Taitel & Dukler (1976), Kordyban (1977) and Mishima & Ishii (1980) enhanced the gas term by dividing it by $K_1 = 0.5$ and $1 - \tilde{H}$, 0.49 and 0.74 respectively. In view of the present analyses, the relative contribution of the gas or liquid destabilizing terms depends on a variety of parameters and operational conditions. Stability analyses which ignore the mobility of the liquid phase and account for the gas destabilizing effects are basically erroneous. In the extremes, however, of definite "*liquid-controlled*" or "*gas-controlled*" transitional zones, empirical constants can be utilized to simplify the general predictive transitional criteria, provided that they are employed on the really dominating contribution.

5. SUMMARY

The instability characteristics of stratified gas–liquid inclined flows are derived along two main routes: stability and well-posedness analyses, and their relations to the stability of kinematic and dynamic waves. In general, the conditions of unstable dynamic waves or ill-posedness are sufficient to indicate instability, while the conditions for the stable dynamic waves or well-posedness are necessary, but insufficient, to assume stability. It is shown that flow pattern transitions are to be established in view of integrated considerations of stability and well-posedness (SWP map).

The physical interpretation of the well-posedness criterion as an upper bound to the stratified flow configuration has been established. Its identity to the classical (inviscid) K–H condition explains the apparant relevance of the frequently applied inviscid analyses for predicting flow pattern transitions in two-phase viscid flows.

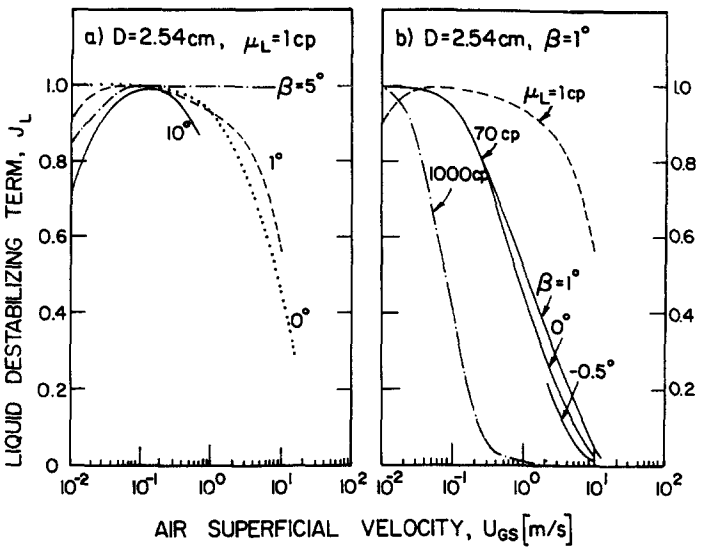

Figure 9. Relative liquid destabilizing contribution—effect of flow inclination and liquid viscosity.

Downward inclination affects, in general, extensions of the well-posed region, while it reduces the stable smooth stratified zones (as defined by the ZNS boundaries). This results in increased "buffer" zones and implies that the stratified wavy pattern become dominant. In this case, whether the waves will trigger flow pattern transition depends on the relative liquid layer thickness in the "buffer" region. In upward inclination also the well-posed region is reduced significantly, whereby only limited (bell-shaped) areas of possible stable stratification are obtained.

In exploring the relative destabilizing contribution of the gas and liquid phases along the ZNS line, it has been found that the departure from a stratified smooth to a slug flow pattern is practically "liquid-controlled" in horizontal and downward inclined air–water systems.

REFERENCES

ANDREUSSI, P. & PERSEN, L. N. 1987 Stratified gas–liquid flow in downwardly inclined pipes. *Int. J. Multiphase Flow* **13,** 565–575.

ANDRITSOS, N. & HANRATTY, T. J. 1987 Interfacial instabilities for horizontal gas–liquid flows in pipelines. *Int. J. Multiphase Flow* **13,** 583–603.

ANDRITOS, N., WILLIAMS, L. & HANRATTY, T. J. 1989 Effect of liquid viscosity on the stratified-slug transition in horizontal pipe flow. *Int. J. Multiphase Flow* **15,** 877–892.

BRAUNER, N. 1990 On the relations between two-phase flow under reduced gravity and earth experiments. *Int. Commun. Heat Mass Transfer* **17,** 271–282.

BRAUNER, N. & MOALEM MARON, D. 1989. Two-phase liquid–liquid stratified flow. *Physico-Chem. Hydrodynam.* **11,** 487–506.

BRAUNER, N. & MOALEM MARON, D. 1991 Analysis of stratified/nonstratified transitional boundaries in horizontal gas–liquid flows. *Chem. Engng Sci.* **46,** 1849–1859.

BRAUNER, N. & MOALEM MARON, D. 1992a Stability analysis of stratified liquid–liquid horizontal flow. *Int. J. Multiphase Flow* **18,** 103–121.

BRAUNER, N. & MOALEM MARON, D. 1992b Flow pattern transitions in two phase liquid–liquid horizontal tubes. *Int. J. Multiphase Flow* **18,** 123–140.

BRAUNER, N. & MOALEM MARON, D. 1992c Identification of the range of "small diameters" conduits, regarding two-phase flow pattern transitions. *Int. Commun. Heat Mass Transfer* **1,** 29–39.

HANRATTY, T. J. 1987 Gas–liquid flow in pipelines. *PhysicoChem. Hydrodynam.* **9,** 101–114.

KORDYBAN, E. S. 1977 Some characteristics of high waves in closed channels approaching Kelvin–Helmholtz instability. *ASME Jl Fluids Engng* **99,** 339–346.

KORDYBAN, E. S. & RANOV, T. 1970 Mechanism of slug formation in horizontal two-phase flow. *J. Bas. Engng* **92,** 857–864.

LIN, P. Y. & HANRATTY, T. J. 1986 Prediction of the initiation of slugs with linear stability theory. *Int. J. Multiphase Flow* **12,** 79–98.

MANDHANE, J. M., GREGORY, G. A. & AZIZ, K. 1974 A flow pattern map for gas–liquid flow in horizontal pipes. *Int. J. Multiphase Flow* **1,** 537–553.

MISHIMA, K. & ISHII, M. 1980 Theoretical prediction of onset of horizontal slug flow. *Trans. ASME Jl Fluids Engng* **102,** 441–445.

SHOHAM, O. 1982 Flow pattern transitions and characterization in gas–liquid two-phase flow in inclined pipes. Ph.D. Dissertation, Tel-Aviv Univ., Ramat-Aviv, Israel.

TAITEL, Y. & DUKLER, A. E. 1976 A model for predicting flow regime transitions in horizontal and near horizontal gas–liquid flow. *AIChE Jl* **22,** 47–55.

WALLIS, G. B. 1969 *One-dimensional Two-phase Flow.* McGraw Hill, New York.

WALLIS, G. B. & DOBSON, J. E. 1973 The onset of slugging in horizontal stratified air–water flow. *Int. J. Multiphase Flow* **1,** 173–193.

WU, H. L., POTS, B. F. M., HOLLENBURG, J. F. & MEERHOFF, R. 1987 Flow pattern transitions in two-phase gas-condensation flow at high pressures in an 8-inch horizontal pipe. Presented at the *3rd Int. Conf. of Multiphase Flow*, The Hague, The Netherlands.